NOTES AND CORRESPONDENCE

Momentum Flux Spectrum of Convectively Forced Gravity Waves: Can Diabatic Forcing Be a Proxy for Convective Forcing?

HYE-YEONG CHUN AND IN-SUN SONG

Department of Atmospheric Sciences, Yonsei University, Seoul, South Korea

TAKESHI HORINOUCHI

Research Institute for Sustainable Humanosphere, Kyoto University, Kyoto, Japan

(Manuscript received 10 September 2004, in final form 12 May 2005)

ABSTRACT

The momentum flux of convectively forced internal gravity waves is calculated using explicitly resolved model-simulated gravity wave data. The momentum flux in a control simulation with nonlinearity and cloud microphysical processes is compared with that in quasi-linear dry simulations with either diabatic forcing or nonlinear forcing. It is found that the momentum flux induced by either of these two sources is significantly different from each other and also from the momentum flux in the control simulation. This is because the spectral distribution and magnitude of each wave source are significantly different and the cancellation of the momentum flux by cross-correlation terms between the two sources cannot be included in the momentum flux by a single source. This suggests that a parameterization of convectively forced gravity waves must take into account nonlinear forcing as well as diabatic forcing in order to qualitatively and quantitatively represent the reference-level momentum flux spectrum.

1. Introduction

Deposition of momentum by the breaking and dissipation of gravity waves is important for large-scale circulation in the middle atmosphere (Lindzen 1981; Garcia and Solomon 1985). Especially nonstationary gravity waves contribute significantly to the momentum budget of the stratosphere and mesosphere. Among various sources in the troposphere, cumulus convection is believed to be a major source of nonstationary gravity waves. In the Tropics, a large fraction of the waves generated by cumulus clouds have high frequencies and they contribute significantly to the momentum forcing required for driving the quasi-biennial oscillation and semiannual oscillation (Dunkerton 1997; Hamilton 1998).

Compared with mountain-induced gravity waves, it is not straightforward to understand how convective sources generate gravity waves. In the literature, three generation mechanisms (thermal forcing, obstacle, and mechanical oscillator mechanisms) have been proposed (Lane et al. 2001, see the references therein). The first two mechanisms consider convective clouds as thermal forcings that generate gravity waves in a stably stratified environment. The difference between the thermal forcing and obstacle mechanisms is that a nonzero background flow relative to the moving convective source is required for the obstacle mechanism, as in the mountain waves. The third mechanism is different from the first two in that convective updrafts stimulate the stably stratified stratosphere and generate gravity waves above clouds. From mesoscale numerical simulations, Lane et al. (2001) suggested dominancy of the mechanical oscillator mechanism based on the magnitude of the nonlinear forcing, representing the mechanical oscillator mechanism, compared with thermal forcing.

Recently, however, Song et al. (2003, SCL hereafter) showed that the wave generation mechanisms cannot

Corresponding author address: Prof. Hye-Yeong Chun, Department of Atmospheric Sciences, Yonsei University, Shinchon-dong, Seodaemun-ku, Seoul 120-749, South Korea.
E-mail: chy@atmos.yonsei.ac.kr

be understood accurately without examining the vertical propagation condition of the gravity waves. The effective forcing that is filtered by a wave propagation condition in the spectral domain can generate gravity waves that reach the stratosphere. Even though the magnitude of the nonlinear forcing is larger than that of the thermal forcing, the effective nonlinear and effective thermal forcings are comparable and largely out of phase with each other. SCL showed that the important scientific point in generation of convective gravity waves is to understand the wave sources and wave propagation condition rather than to simply identify the dominant generation mechanism based on the magnitude of wave sources without considering the wave filtering effect.

The spectral distribution of gravity wave momentum flux at a reference level is a crucial factor in gravity wave drag (GWD) parameterization. However, most current spectral GWD parameterization schemes assume a certain spectral distribution at a fixed launching level without considering wave sources explicitly. Recently, spectral parameterizations including explicit treatment of convective sources have been proposed by Beres et al. (2004), Beres (2004), and Song and Chun (2005, SC05 hereafter). These studies analytically formulated cloud-top momentum flux using linear internal gravity waves induced by a specified diabatic forcing that has a Gaussian-type structure in time and space. The first two consider a uniform wind and stability condition, while the third includes a constant shear in the convective region and a stability difference between the convective region and above, representing a favorable condition for midlatitude squall lines as used in numerical simulations by SCL. The momentum flux formulation at the reference level (cloud top) was validated using explicitly calculated convective gravity waves in mesoscale numerical simulations: for a two-dimensional case in Beres et al. (2004) and for both two- and three-dimensional cases in SC05. Though both studies showed that the formulation represents reasonably well the simulated results, some discrepancies are discussed in SC05. The major reason for such discrepancies, besides simplicity of the analytical model compared with the numerical model that includes nonlinearity and cloud microphysics, is likely the neglect of the nonlinear forcing that contributes significantly to the momentum flux spectrum in the high phase speed range.

In this study, an attempt is made to determine the extent to which the momentum flux spectrum from a single source represents the convective momentum flux and, consequently, to assess the reliability of parameterization of wave momentum flux based on diabatic forcing alone. For this, we revisit SCL and calculate the momentum flux spectrum of gravity waves induced by each wave source, and compare it with a control simulation including nonlinear and moist processes. To understand the simulated momentum flux spectrum, analytical formulation of the momentum flux induced by two sources is derived (section 2). We calculate the spectral distribution of each wave source (section 3) and finally discuss implications and future work for parameterization of convective gravity waves (section 4).

2. Momentum flux spectrum of gravity waves induced by each wave source

In the present study, all results are based on the numerical simulations by SCL. The numerical simulations of convectively forced internal gravity waves in SCL were conducted using a two-dimensional version of the Advanced Regional Prediction System (ARPS) (Xue et al. 1995), which is a nonhydrostatic, compressible model with explicit liquid–ice phase cloud microphysical processes. Two types of numerical simulations were performed: a control simulation (CTL) including nonlinearity and cloud microphysical processes, and three quasi-linear dry simulations forced by nonlinear momentum forcing (DRYM), nonlinear momentum and heat flux forcing (DRYMH), and diabatic forcing (DRYQ). The forcings for the quasi-linear dry simulations are defined through the process of linearization of the ARPS model under anelastic approximation [Eqs. (8)–(19) of SCL] and they are calculated from the result of the CTL simulation and saved at 1-min intervals. All numerical simulations are conducted for 12 h in a physical domain of 1100 km and 35 km in zonal and vertical directions, respectively. Since the DRYMH simulation includes all nonlinear forcing terms, the DRYMH and DRYQ simulations are considered in the present study. Detailed description of the numerical simulations can be found in SCL.

Figure 1 shows the momentum flux spectrum ($\overline{\bar{\rho}u'w'}$) at $z = 18$ km for the CTL, DRYQ, DRYMH simulations and for DRYQ + DRYMH. The momentum flux of DRYQ + DRYMH is calculated by wind perturbations that are summed up from the DRYMH and DRYQ simulations. That is, $w'_{\mathrm{DRQ+DRYMH}} = w'_{\mathrm{DRYQ}} + w'_{\mathrm{DRYMH}}$ and $u'_{\mathrm{DRQ+DRYMH}} = u'_{\mathrm{DRYQ}} + u'_{\mathrm{DRYMH}}$. The bottom two panels represent the momentum fluxes by cross-correlation terms between the wind perturbation in the DRYMH and DRYQ simulations. Several interesting features can be found in Fig. 1. First, the spectral distribution of the momentum flux by either the DRYMH or DRYQ simulation is significantly different from the CTL simulation. In DRYQ, the major spectral

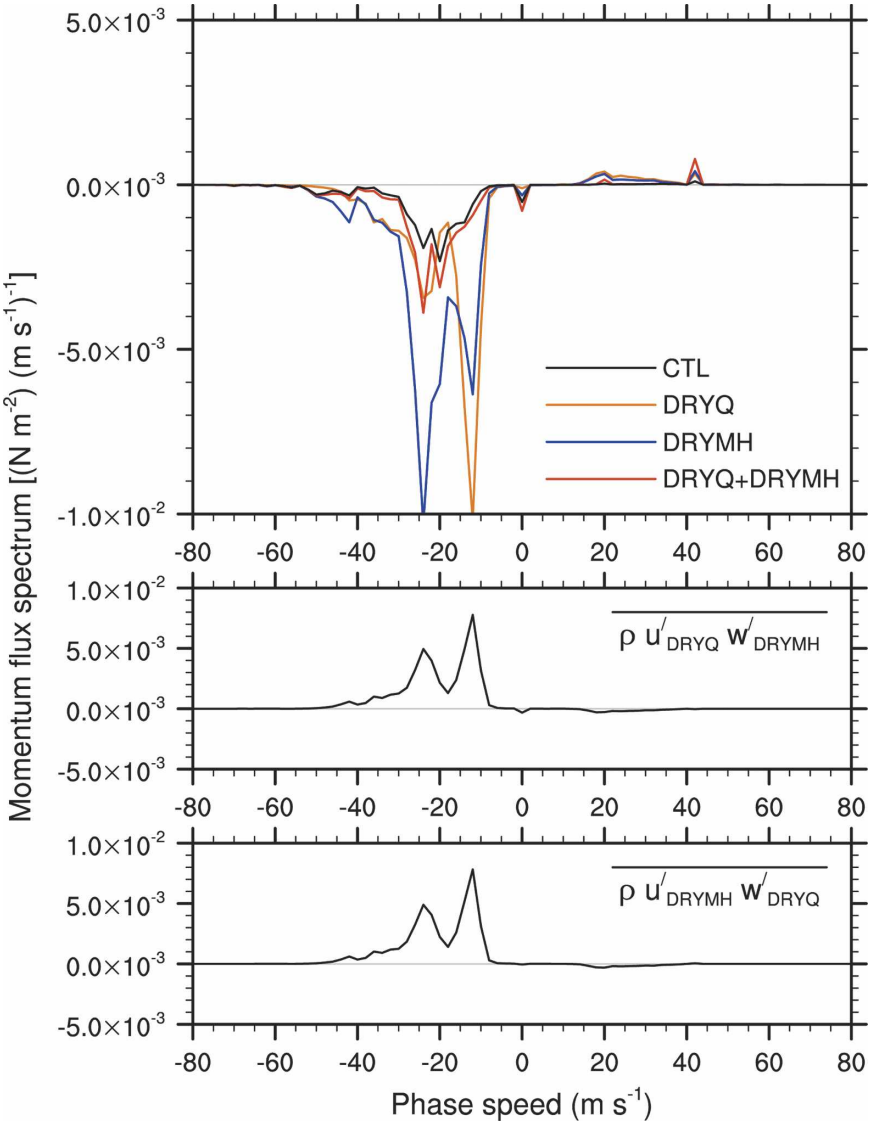

FIG. 1. Momentum flux spectra of gravity waves induced by the (upper) CTL, DRYQ, DRYMH, and DRYQ + DRMH simulations and by (middle and lower) cross-correlation terms in Eq. (1). Numerical simulations of the CTL, DRYQ, DRYMH, and DRYQ + DRYMH are explained in the text.

peak exists at $c = -12$ m s^{-1} with a secondary peak at $c = -24$ m s^{-1}, while in DRYMH the major peak exists at $c = -24$ m s^{-1} with a secondary peak at $c = -12$ m s^{-1}. None of the two matches CTL, which has its primary peak at $c = -20$ m s^{-1} and a secondary peak at –24 m s^{-1}. Second, the magnitude difference of the momentum flux between CTL and either DRYMH or DRYQ is more significant than that between the latter two. The maximum magnitude of the momentum flux by either DRYQ or DRYMH is almost one order of magnitude larger than that of CTL. On the other hand, the shapes of the spectra for all simulations are similar for $c > -5$ m s^{-1} and $c < -55$ m s^{-1}, with slightly different magnitudes. Third, the momentum flux in DRYQ + DRYMH is similar to that of CTL, except for the range of -24 m s$^{-1} < c < -20$ m s^{-1} in which the quasi-linear simulations cannot take into account the nonlinear interaction in the CTL simulation, as shown by SCL (Figs. 8 and 10 of SCL). Fourth, in the phase speed range of -28 m s$^{-1} < c < -18$ m s^{-1}, the momentum flux of DRYQ represents reasonably well the momentum flux of DRYQ + DRYMH.

Considering that the momentum flux of DRYQ + DRYMH is reasonably comparable to that of CTL,

while the momentum flux of either DRYMH or DRYQ is much larger than that of CTL, the momentum flux of the cross-correlation terms must have different signs. This can be expressed by a simple calculation:

$$\begin{aligned}\overline{\bar{\rho}u'_{\mathrm{DRYQ+DRYMH}}w'_{\mathrm{DRYQ+DRYMH}}} &= \overline{\bar{\rho}u'_{\mathrm{DRYQ}}w'_{\mathrm{DRYQ}}} + \overline{\bar{\rho}u'_{\mathrm{DRYMH}}w'_{\mathrm{DRYMH}}} \\ &\quad + \overline{\bar{\rho}u'_{\mathrm{DRYQ}}w'_{\mathrm{DRYMH}}} + \overline{\bar{\rho}u'_{\mathrm{DRYMH}}w'_{\mathrm{DRYQ}}}. \end{aligned} \quad (1)$$

The term on the left-hand side of (1) and the first two terms on the right-hand side of (1) are shown in the upper panel of Fig. 1 as DRYQ + DRYMH, DRYQ, and DRYMH, respectively, while the third and fourth terms on the right-hand side of (1) are shown at the middle and lower panels, respectively. This shows that the magnitude of the momentum flux by cross-correlation terms is large with positive sign, and the two spectral peaks ($c = -12$ and -24 m s^{-1}) exist at which the primary peaks in the DRYQ and DRYMH simulations, respectively, are located.

It is interesting to observe in Fig. 1 that the cross-correlated momentum fluxes are almost identical in their magnitude and spectral shape, with a sign that is different from the momentum flux by the single source. To get some insight into this result, we derive an analytical expression of cross-correlated momentum flux induced by two separate forcings.

Let u' and w' be the zonal and vertical components of a monochromatic gravity wave in a two-dimensional framework given by

$$\begin{aligned} u'(x, z, t) &= \mathrm{Re}[\tilde{u}(k, \omega)e^{z/2H}e^{i(kx+mz-\omega t)}] \\ &= \frac{1}{2}e^{z/2H}(\tilde{u}e^{i\psi} + \tilde{u}^*e^{-i\psi}), \end{aligned} \quad (2a)$$

$$\begin{aligned} w'(x, z, t) &= \mathrm{Re}[\tilde{w}(k, \omega)e^{z/2H}e^{i(kx+mz-\omega t)}] \\ &= \frac{1}{2}e^{z/2H}(\tilde{w}e^{i\psi} + \tilde{w}^*e^{-i\psi}), \end{aligned} \quad (2b)$$

where k and m are the horizontal and vertical wavenumbers, respectively, ω is the frequency, H is the scale height of the basic-state density, ψ is the wave phase ($=kx + mz - \omega t$), and $\tilde{u}^*(\tilde{w}^*)$ is the complex conjugate of $\tilde{u}(\tilde{w})$. In SCL, it was shown that the anelastic approximation can be applied to the gravity waves and their forcing terms. Therefore, u' and w' in (2) are related through the anelastic continuity equation as

$$\frac{\partial}{\partial x}(\bar{\rho}u') + \frac{\partial}{\partial z}(\bar{\rho}w') = 0, \quad (3)$$

where the basic-state density $\bar{\rho}$ is assumed to be $\bar{\rho}(z) = \rho_0 e^{-z/H}$. Using (2) and (3), one can obtain the following relationship between $\tilde{u}$ and $\tilde{w}$:

$$ik\tilde{u} = \left(\frac{1}{2H} - im\right)\tilde{w}. \quad (4)$$

We now assume that u'_1 and u'_2 (w'_1 and w'_2) are the zonal (vertical) wind perturbations induced by two sources, respectively. Then, $u'_1w'_2$ and $u'_2w'_1$ averaged over a horizontal wavelength can be written as

$$\begin{aligned}\overline{u'_1w'_2} = -\frac{1}{4k}e^{z/H}\Bigg[&\left(m + \frac{i}{2H}\right)\tilde{w}_1\tilde{w}_2^* \\ &+ \left(m - \frac{i}{2H}\right)\tilde{w}_1^*\tilde{w}_2\Bigg], \end{aligned} \quad (5a)$$

$$\begin{aligned}\overline{u'_2w'_1} = -\frac{1}{4k}e^{z/H}\Bigg[&\left(m + \frac{i}{2H}\right)\tilde{w}_2\tilde{w}_1^* \\ &+ \left(m - \frac{i}{2H}\right)\tilde{w}_2^*\tilde{w}_1\Bigg]. \end{aligned} \quad (5b)$$

To demonstrate the phase relationships between the waves induced by each source, $\tilde{w}_1$ and $\tilde{w}_2$ are set to $|\tilde{w}_1|e^{i\phi_1}$ and $|\tilde{w}_2|e^{i\phi_2}$. Then, the cross-correlated momentum fluxes are

$$\overline{\bar{\rho}u'_1w'_2} = -\rho_0\frac{1}{2k}|\tilde{w}_1||\tilde{w}_2|\,\mathrm{Re}\left[\left(m + \frac{i}{2H}\right)e^{i(\phi_1 - \phi_2)}\right], \quad (6a)$$

$$\overline{\bar{\rho}u'_2w'_1} = -\rho_0\frac{1}{2k}|\tilde{w}_1||\tilde{w}_2|\,\mathrm{Re}\left[\left(m + \frac{i}{2H}\right)e^{-i(\phi_1 - \phi_2)}\right]. \quad (6b)$$

In the case where the vertical wavelength of gravity waves in the stratosphere is much less than $4H\pi$ (equivalently, to make the Boussinesq approximation), the second terms inside the last parentheses in (6a) and (6b) can be neglected. In that case, the two cross-correlated momentum fluxes are identical. This approximation is reasonable in the present simulation by SCL, given that the dominant vertical wavelengths of vertical velocity perturbation in the stratosphere range roughly from 6.6 to 9.9 km in all simulations, and they are much less than $4H\pi$ ($\sim$79 km, with $H = 6.3$ km used in SCL). This explains why the cross-correlated momentum fluxes in Fig. 1 are nearly identical.

The sign of the cross-correlated momentum flux is determined by $\phi_1 - \phi_2$, the phase difference between w'_1 and w'_2. When $|\phi_1 - \phi_2| < \pi/2$, then $\cos(\phi_1 - \phi_2)$ is positive, and the cross-correlated momentum flux has

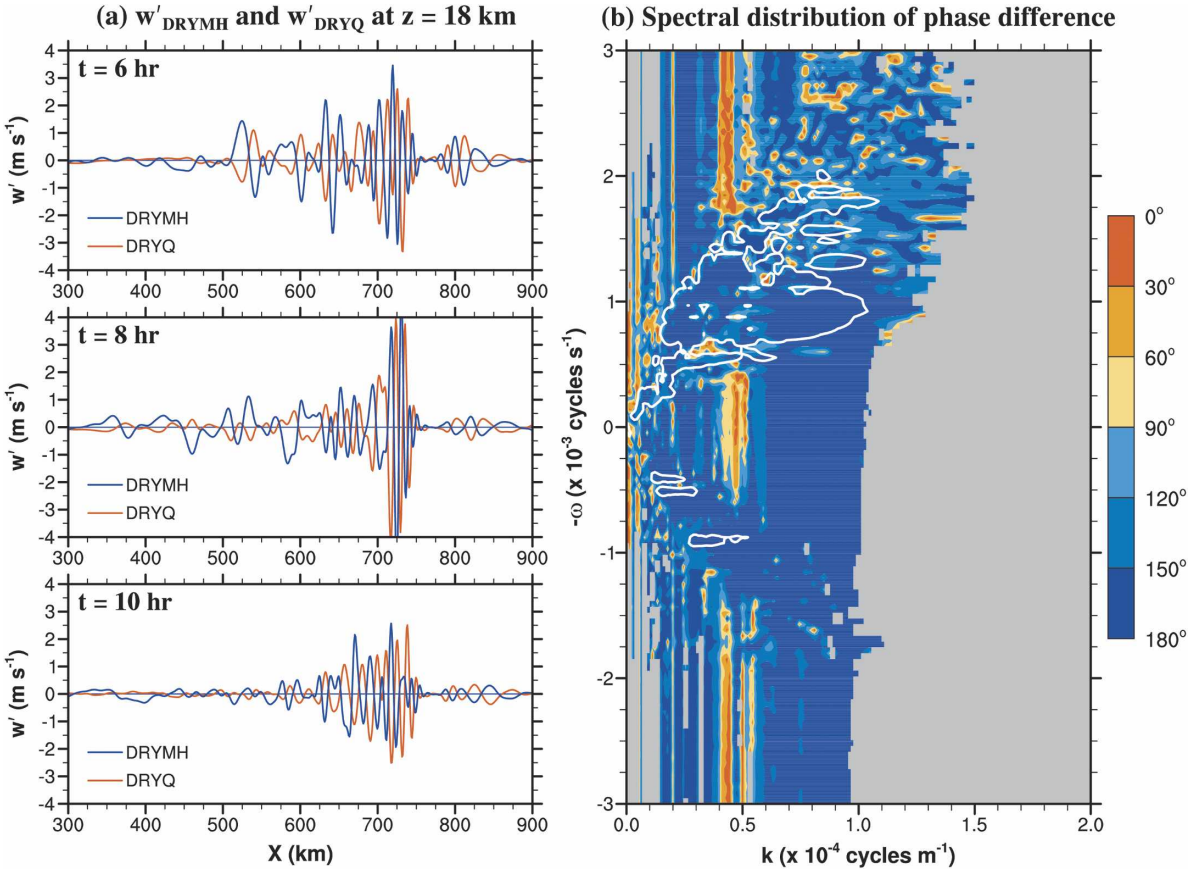

FIG. 2. (a) Horizontal distribution of vertical velocity at $z = 18$ km and $t = 6$, 8, and 10 h for the DRYQ (red lines) and DRYMH (blue lines) simulations, and (b) spectral distribution of the phase difference (degrees) between w'_{DRYQ} and w'_{DRYMH} (shading) in horizontal wavenumber and frequency domain. White contours in (b) denote the amplitude spectrum between w'_{DRYQ} and w'_{DRYMH} of 5×10^5 m^2 s^{-2} (cycles m^{-1})$^{-1}$ (cycles s^{-1})$^{-1}$. The phase difference is not plotted in the spectral regions (gray shading) where the amplitude spectrum is less than 5×10^2 m^2 s^{-2} (cycles m^{-1})$^{-1}$ (cycles s^{-1})$^{-1}$.

the same sign as the momentum flux by a single source, which can be derived directly from (6) as

$$\overline{\rho u_1' w_1'} = -\rho_0 \frac{m}{2k} |\tilde{w}_1|^2, \tag{7a}$$

$$\overline{\rho u_2' w_2'} = -\rho_0 \frac{m}{2k} |\tilde{w}_2|^2. \tag{7b}$$

When $\pi/2 < |\phi_1 - \phi_2| \leq \pi$, then $\cos(\phi_1 - \phi_2)$ is negative, and the cross-correlated momentum flux has the opposite sign from the momentum flux by a single source. This result implies that cross-correlated momentum fluxes can either cancel out or increase the momentum fluxes by each forcing, and the degree of cancellation or increase depends on the phase difference between the waves induced by two separate sources.

In the present simulation, $k > 0$, $\omega < 0$, and $m > 0$ for the westward and upward propagating waves. Therefore, the momentum flux of westward propagating waves (with negative phase speeds in Fig. 1) induced by each forcing is negative. Since the cross-correlated momentum flux as shown in Fig. 1 is positive, the vertical velocity perturbation induced by two sources in the present simulations must be negatively correlated with each other. To examine this, the horizontal distribution of vertical wind perturbations for the DRYQ and DRYMH simulations at $z = 18$ km and $t = 6$, 8, and 10 h (Fig. 2a) and spectral distribution of the phase difference (in degrees) between w'_{DRYQ} and w'_{DRYMH} at $z = 18$ km (Fig. 2b) are calculated. The white contours in Fig. 2b denote the amplitude spectrum between the two perturbations of 5×10^5 m^2 s^{-2} (cycles m^{-1})$^{-1}$ (cycles s^{-1})$^{-1}$, and the phase difference is not plotted in the spectral regions (gray shading) where the amplitude spectrum is less than 5×10^2 m^2 s^{-2} (cycles m^{-1})$^{-1}$ (cycles s^{-1})$^{-1}$. The amplitude spectrum is defined as $\sqrt{\mathrm{CO}^2(k, \omega) + \mathrm{Q}^2(k, \omega)}$, where CO and Q are the cospectrum and quadrature spectrum between w'_{DRYQ} and w'_{DRYMH} at $z = 18$ km, respectively. The phase differ-

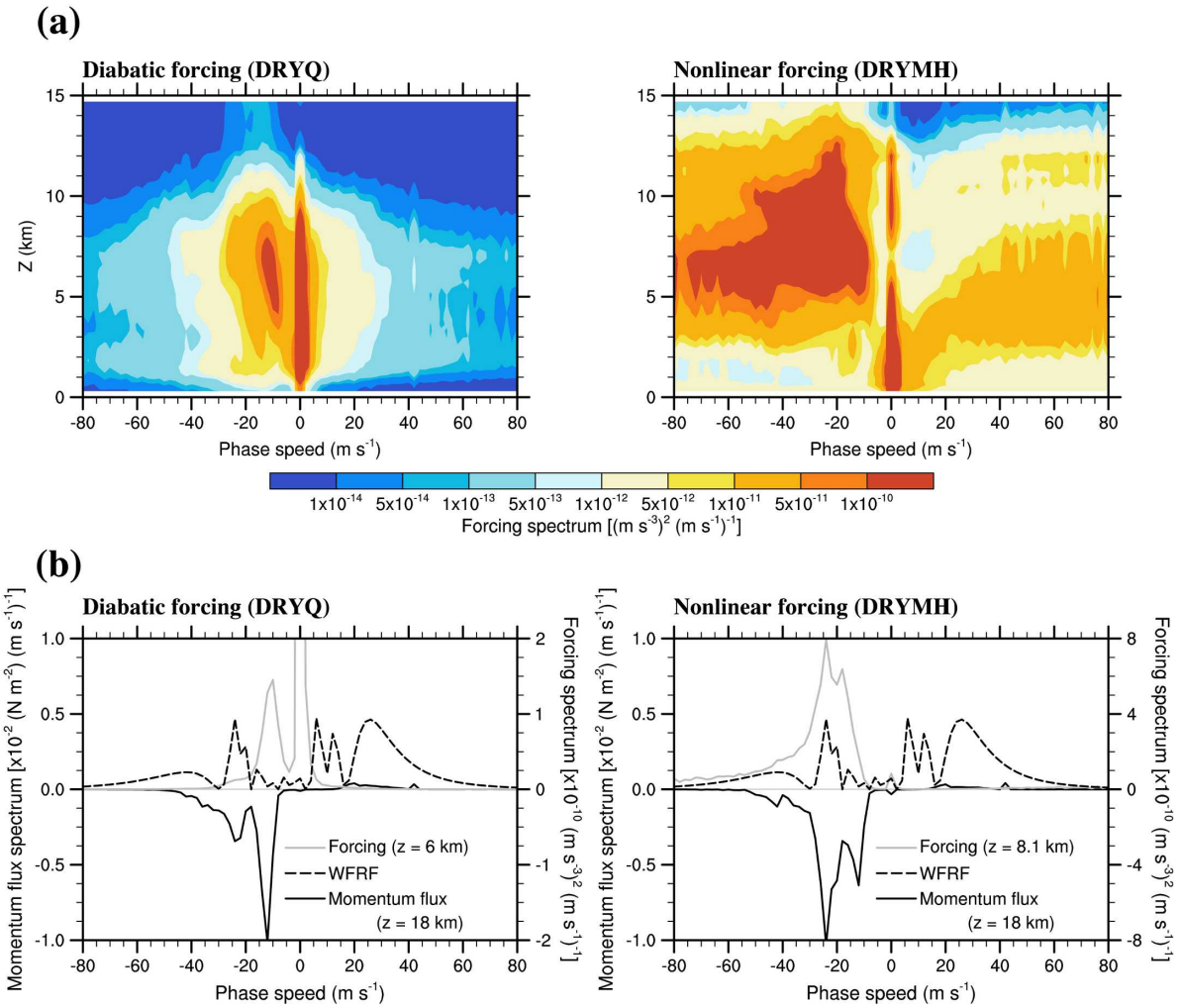

FIG. 3. (a) Power spectrum of the (left) diabatic forcing and (right) nonlinear forcing used for the DRYQ and DRYMH simulations, respectively, and (b) spectral distributions of diabatic forcing at $z = 6$ km and nonlinear forcing at $z = 8.1$ km along with the wave filtering and resonance factor (WFRF) superimposed on the momentum flux at $z = 18$ km by (left) DRYQ and (right) DRYMH simulations, respectively, as shown in Fig. 1.

ence is calculated as $(180°/\pi)\cos^{-1}(\mathrm{CO}/\sqrt{\mathrm{CO}^2 + \mathrm{Q}^2})$. The two perturbations have relatively strong spectral components in spectral regions enclosed by the contours, and therefore the phase difference is less meaningful outside of those spectral regions. Negative phase relationship between the two simulations is evident in the vertical wind perturbation throughout the simulations (Fig. 2a) and in most spectral regions (Fig. 2b) with two peaks ($c = -12$ and -24 m s^{-1}) at which the cross-correlated momentum fluxes have spectral peaks.

3. Spectrum of wave sources and their contribution to the momentum flux

Figure 1 shows that the momentum flux induced by each wave source is significantly different from each other. As shown in (7), the difference in the momentum flux spectrum induced by each source is primarily due to the wave amplitude spectrum ($|\tilde{w}_1|$ and $|\tilde{w}_2|$). Since the wave amplitude spectrum must be related to source spectrum, it is worth to investigate each source spectrum. Figure 3a shows the power spectrum density of the diabatic forcing (left panels) and nonlinear forcing (right panels) used in the DRYQ and DRYMH simulations. The spectral distribution of each forcing is significantly different from each other. The diabatic forcing is concentrated near $c = 0$ with a secondary peak near -12 m s^{-1} and is confined below about $z = 12$ km. The nonlinear forcing, on the other hand, has strong powers in a broad phase speed range ($c < -10$ m s^{-1}) and is occupied by the whole forcing depth (15 km). Also, the nonlinear forcing for $c > 10$ m s^{-1} below

about $z = 8$ km has stronger powers than the diabatic forcing.

The spectral distribution of the forcing alone, however, is not likely to explain the spectral distribution of momentum flux shown in Fig. 1. Even though the diabatic forcing has the primary peak at $c = 0$ and a secondary peak at $c = -12$ m s^{-1}, the momentum flux of DRYQ has the primary peak at $c = -12$ m s^{-1} and a secondary peak at $c = -24$ m s^{-1}. This is also true for the nonlinear forcing in which a relatively strong power near $c = 0$ is not used to generate momentum flux at $z = 18$ km. SC05, based on analytical formulation, showed that the momentum flux above convection is determined by the spectral combination of wave source and a wave filtering and resonance factor (WFRF) [(19) of SC05]. The WFRF represents wave filtering (critical-level filtering and vertical propagation constraint) and resonance between the vertical harmonics consisting of forcing and natural wave modes with vertical wavenumbers given by the dispersion relationship.

Figure 3b shows the spectrum of the diabatic (nonlinear) forcing at $z = 6$ km (8.1 km) and WFRF superimposed on the momentum flux spectrum of the DRYQ (DRYMH) simulation on the left (right) panel. Very weak momentum flux near $c = 0$ in DRYQ, regardless of strong forcing there, is due to very small value of WFRF. The primary ($c = -12$ m s^{-1}) and the secondary ($c = -24$ m s^{-1}) peaks in the momentum flux of DRYQ are mainly due to strong forcing and large value of WFRF, respectively. In DRYMH, the primary peak ($c = -24$ m s^{-1}) of the momentum flux is due to the overlapping of strong forcing and large value of WFRF, while the secondary peak ($c = -12$ m s^{-1}) is due to relatively strong forcing there. Overall, the shape and magnitude of the momentum flux spectrum are determined by spectral combination of the forcing and WFRF, according to a degree of overlapping between the two. There is, however, a phase speed range ($c < -50$ m s^{-1}) in which the momentum flux of DRYMH cannot be well explained by spectral combination of the forcing and WFRF in Fig. 3b (right panel). One possible reason is that the vertical profile of the forcing used to calculate WFRF, a second-order polynomial with a maximum value at the center, does not represent the nonlinear forcing well, while it represents relatively well the diabatic forcing.

4. Summary and discussion

The momentum flux spectra of convectively forced internal gravity waves, explicitly calculated by SCL using a high-resolution mesoscale model, were calculated for the CTL simulation including nonlinearity and moist microphysical processes and for two quasi-linear dry simulations forced by diabatic forcing (DRYQ) and nonlinear momentum and heat flux forcing (DRYMH). It showed that the momentum flux spectrum induced by either of the forcings is significantly different from each other and from that of the CTL simulation. In some phase speed ranges, magnitude of the momentum flux by the single forcing is almost one order of magnitude larger than that of the CTL simulation, even though momentum flux by DRYQ + DRYMH is reasonably comparable to that of CTL. This is because spectral distribution and magnitude of each wave source are significantly different from each other and the cancellation of the momentum flux by cross-correlation terms between the two sources cannot be included in the momentum flux by a single source.

The result of the present study has important implications for convective gravity wave parameterization. It indicates that the momentum flux spectrum induced by either of the forcings cannot appropriately represent the convective gravity waves in the major forcing region. In the simulation presented here, the momentum flux induced by the diabatic forcing presents reasonably well the momentum flux by the total forcing only in the range of -28 m s$^{-1} < c < -18$ m s^{-1}. This suggests that a parameterization of convective gravity waves must take into account both forcing mechanisms in order to qualitatively and quantitatively represent the reference-level momentum spectrum. Therefore, the new attempts (by Beres et al. 2004; Beres 2004; SC05) to formulate the momentum flux spectrum of convective gravity waves induced by diabatic source alone need further improvement, although they are still much more realistic than the spectral gravity wave drag parameterization used in current large-scale models that have a prescribed source spectrum.

The major improvement is likely to include the nonlinear forcing in addition to the diabatic forcing in the parameterization. Since the nonlinear and diabatic forcings are independent in a governing equation of internal gravity waves, it is generally possible to obtain a linear solution of gravity waves induced by both forcings and resultant momentum flux spectrum. However, one of the main problems, besides additional efforts on mathematical treatment, is that we do not know much about the spatial and temporal structure of the nonlinear forcing, compared with the diabatic forcing that is relatively well known through observational and numerical modeling studies. Also, more importantly, the nonlinear forcing and diabatic forcing are not independent but are somehow coupled with each other. Therefore, if we simply put a nonlinear forcing in the formulation without enough knowledge of forcing structure

and its relationship with the diabatic forcing, extra uncertainties will be added to the formulation. Systematic numerical simulations are currently under way to find the structure of the nonlinear forcing and a relationship with the diabatic forcing.

Acknowledgments. The authors thank three anonymous reviewers for their careful reading of the manuscript and helpful comments. This study was partially conducted when the first author was visiting Research Institute for Sustainable Humanosphere (RISH) at Kyoto University during her sabbatical leave. This work was supported by R02-2004-000-10027-0 from the Basic Research Program of the Korea Science and Engineering Foundation and by the Ministry of Science and Technology of Korea through the National Research Laboratory Program.

REFERENCES

Beres, J. H., 2004: Gravity wave generation by a three-dimensional thermal forcing. *J. Atmos. Sci.,* **61,** 1805–1815.

——, M. J. Alexander, and J. R. Holton, 2004: A method of specifying the gravity wave spectrum above convection based on latent heating properties and background wind. *J. Atmos. Sci.,* **61,** 324–337.

Dunkerton, T. J., 1997: The role of gravity waves in the quasi-biennial oscillation. *J. Geophys. Res.,* **102,** 26 053–26 076.

Garcia, R. R., and S. Solomon, 1985: The effect of breaking gravity waves on the dynamics and chemical-component of the mesosphere and lower thermosphere. *J. Geophys. Res.,* **90,** 3850–3868.

Hamilton, K., 1998: Effects of an imposed quasi-biennial oscillation in a comprehensive troposphere–stratosphere–mesosphere general circulation model. *J. Atmos. Sci.,* **55,** 2393–2418.

Lane, T. P., M. J. Reeder, and T. L. Clark, 2001: Numerical modeling of gravity wave generation by deep tropical convection. *J. Atmos. Sci.,* **58,** 1249–1274.

Lindzen, R. S., 1981: Turbulence and stress owing to gravity waves and tidal breakdown. *J. Geophys. Res.,* **86,** 9709–9714.

Song, I.-S., and H.-Y. Chun, 2005: Momentum flux spectrum of convectively forced internal gravity waves and its application to gravity wave drag parameterization. Part I: Theory. *J. Atmos. Sci.,* **62,** 107–124.

——, ——, and T. P. Lane, 2003: Generation mechanisms of convectively forced internal gravity waves and their propagation to the stratosphere. *J. Atmos. Sci.,* **60,** 1960–1980.

Xue, M., K. Droegemeier, V. Wong, A. Shapiro, and K. Brewster, 1995: ARPS Version 4.0 User's Guide. Center for Analysis and Prediction of Storms, University of Oklahoma, 380 pp.